Robustness Improvement for Chipless RFID Reading Using Polarization Separation

Florian Requena, Nicolas Barbot, Darine Kaddour, Etienne Perret

Robustness Improvement for Chipless RFID Reading Using Polarization Separation

Florian Requena, *Student Member, IEEE,* Nicolas Barbot, *Member, IEEE,*
Darine Kaddour, *Member, IEEE,* and Etienne Perret, *Senior Member, IEEE*

***Abstract*—In this paper, a novel method to improve the readability of chipless tags is presented. When the EM wave falls upon the tag's surface at normal incidence or with a known incidence, the proposed approach permits to obtain a higher signal-to-noise ratio (SNR) of resonators whose orientation with respect to the normal to the plane in which the tag is positioned is unknown and thus, to increase the reading distance of the tag. It introduces a technique based on the detection of this tag orientation in relation to the antennas; a projection of the signals will allow to correct this misalignment in order to always be able to decode the tag identifier on a signal that corresponds to an ideal alignment between the tag and the antennas. With this principle, it is also possible to separate the resonance mode of the resonator that is connected to the identifier from other parasitic resonance modes that may appear due to a possible misalignment between the tag and the antenna. This principle is applied to loop resonators commonly used in chipless RFID which can present strong parasitic modes of resonance. Also, this method makes the reading orientation invariant, allowing to read the resonator whatever its orientation with respect to the normal to the plane in which the tag is positioned. Likewise, the proposed method can be also used to sense this resonator orientation. This method requires a dual-polarization antenna and a 2-ports vector network analyzer (VNA). Results are validated in simulation and with real-environment measurements for a single resonator as well as for multiple resonators, as it is classically used in the chipless RFID technology. Measurements in a harsh environment, as well as comparisons with classical techniques such as time gating, are presented. A study on the improvment of the read range is achieved to highligth the potential of the proposed technique. A reading distance of more than 80cm was thus obtained, which represents 20cm more than with the classic use of a post-processor based on time gatting. Finally, the principle of the measurement is generalized by applying it to a tag with a ground plane and considering that the antenna is not necessarily placed in normal incidence with respect to the plane of the tag.**

***Index Terms*—Chipless RFID, Radar, Reading method, Robustness, Scatterer, Sensor.**

I. Introduction

RADIO frequency identification (RFID) is an identification technology based on the use of radio waves. The first applications of this technology date back to the Second World War. It includes the aircraft identification "Friendly or Foe" [1]. This technique consisted of equipping airplanes with a radio frequency transponder allowing them to backscatter a coded signal when the plane was illuminated with an electromagnetic wave. Thus, the infantry on the ground could recover this signal and compare it to a database to judge the hostility of the plane. In parallel, from the beginning of the 1900s until the Cold War, the work of Léon Theremin was also at the origin of the physical concepts which are at the foundation of the RFID technology used today [2]. A passive spying system called "The Great Seal bug" was given as a gift by the USSR to the American embassy during the Cold War period. This passive device was a microphone operating remotly, based on the principle of retro-modulation of radio waves [3].

RFID was then democratized with consumer applications such as anti-theft systems in supermarkets, passport identification, access/transport cards, or even animal identification [4]. The RFID anti-theft system EAS (Electronic article surveillance) in supermarkets was the first major commercial use of RFID technology. Today, several classes of RFID have been developed to answer a large variety of problems [5]. One of them is the chipless RFID technology whose goal is to provide more functionalities than a barcode at a comparable price.

A large number of resonators of different shapes have been introduced in RFID chipless [6], [7]. Contrary to the previous generation of tags that included one or two antennas and a transmission line on which the resonators were positioned [8], the REP approach (for RF Encoding Particle) allows to realize tags where only resonant structures are present [9]. These simpler structures have shown better performances in terms of compactness but also in terms of reading distance in real environments [9]–[11]. Also, as previously indicated, these resonant forms are compatible with reading techniques based on time gating or the polarization of the reading system to significantly increase their performance. Contrary to the so-called time-domain Chipless RFID tags [12], [13], the reading principle of the REP tags is based on the resonance frequency of the geometrical shape that composes the tag. Also, strictly speaking, the information is not obtained from the structure mode and the antenna mode [14] of the tag as for the time-domain tags [13] but from the extraction of the resonance modes of the tag [11], [15]–[18]. Most often, in the operational frequency band of the tag, only one resonance mode per elementary form is present, so the temporal expression of the backscattered electric field is none other than a damped sinusoïdal to which a term is added corresponding to the non-resonant part of the backscattered field and which, from

Manuscript received X; revised X; accepted X. Date of publication X; date of current version X.

This project has received funding from the European Research Council (ERC) under the European Union's Horizon 2020 research and innovation program (grant agreement No 772539). This work is also supported by Univ. Grenoble Alpes.

(Corresponding author: Florian Requena.) The authors are with Univ. Grenoble Alpes, Grenoble INP, LCIS, F-26000 Valence, France.

a temporal point of view, is present only in the early-time response of the tag [11], [15]–[18]. It can be seen from this example that this representation of the electric field is not the one used to describe loaded antennas [14], which means that the terms "structure mode" and "antenna mode" are not strictly adapted to describe the operation of a REP tag. To ease the implementation (especially for sensor applications) and reduce the price of the tag, REP tags without a ground plane are very interesting [9], [10]. Techniques allowing to take into account the frequency shifts observed when such a tag is placed on different supports have been introduced and allow to use these tags in a large number of configurations [19]. We note that the rectangular loop resonators [20], which have a RCS twice as high as the C-loops [7], [9], [19], [20], are particularly interesting shapes because they have a high quality factor (of the order of 130 at 3 GHz), comparable to resonators with a ground plane [6], [21]. On the other hand, the main drawback that limits the use of these structures is the impossibility of reading them in cross-polarization (in this case the loop must be rotated by 45° compared to a classic co-polarization reading). This is directly linked to the fact that a rectangular loop has two resonance modes, namely a weak reasoning mode (parasitic mode) which is located a few MHz before the loop mode, the later one is resonant enough to be used to encode information. It is therefore particularly expected to be able to read these loops with a new approach that will allow to isolate the polarization that contains the information, thus reducing a significant part of the amplitude of the backscattered field (namely the parasitic mode, but more generally the contribution of the reflection oriented in the direction of this mode) which behaves as noise in the measurement of a REP chipless tag. Subsequently, this method is general and allows to improve the reading of all the REP type tags.

One of the direct drawbacks of this approach is the deterioration of the tag readability, for example in terms of reading range compared to a UHF RFID tag. By removing the chip and the load modulation used in classical RFID systems, chipess tag reading is lower and clearly less robust in real environment. However, a certain level of robustness is needed to correctly read the tag, as well as to improve the reading distance. In addition, today chipless RFID applications do not only include the identification functionality but also sensing capabilities [8], [22]–[25]. This sensing approach often relies on the remote measurement of a shift in the resonance frequency of a resonator. Such shifts can be as low as 25 kHz [21], [22], hence a certain level of robustness of reading is highly expected for practical applications of chipless RFID technology.

Several works have been done to improve the robustness reading of chipless RFID. We can cite for example [26], [27] where authors have shown that the arrangement of the resonators on the tag can improve its robustness. Other works are based on the polarization of electromagnetic waves. Indeed, the environment does not usually depolarize electromagnetic waves. For this reason, de-polarizing tags such as in [10], [28] or resonators placed at 45° in relation to the orientation of the antennas have been studied to send a signal with a polarization in a different direction from the environment's response (cross polarization measurments). The drawback of such methods is that only a part of the signal is depolarized by the tag and arrives at the receiving antenna positioned at an angle of 90° regarding the transmitting antenna. Hence the received signal is reduced and so is its readability distance (for example, 6dB is lost when a resonator is placed at 45 degrees with respect to the same measurement in co-polarization with an angle 0 with respect to the antennas). Also, placing resonators at 45° can excite parasitic modes of resonances which can pollute the final electromagnetic response of the resonator. Moreover, in all these measurement approaches, the tag orientation must be known prior to the measurement. This is why measurement techniques independent of the orientation of the tag have recently been introduced from the reader part [29], [30] or the tag part [31]. However, these techniques do not separate the wave reflected by the environment from the one linked to the tag and therefore its identifier [32]. Moreover, numerous approaches based on the postprocessing of the time response of a resonator have been proposed to increase the robustness. We can cite for example methods based on time gating [11], [17], [18]. Even if this method is very effective and allows to significantly improve the performance of reading chipless tags, unfortunately, as with cross-polarization readings, cutting off the signal (early time part) also contributes to not using a significant portion of the energy that contain the tag identifier. In addition to that, possible different attenuation coefficient of resonators on the same tag due to their different working frequencies or their Q-factors as well as the empirical way to obtain the needed parameters (such as t_{start} and t_{stop} to select the part of the time signal to be retained) are majors drawbacks of this technique. Most of the time, these parameters need to be characterized by the user based on the measurement responses.

In terms of application, in a very classical way, we consider a chipless tag attached to the plane surface of an object and the antenna of the reader which points in the direction of the tag. This antenna will be either positioned in the direction normal to the tag plane or positioned in any way as long as it is able to excite the resonance mode of the tag used to encode the information. Finally, we consider in particular the angle of rotation of the tag compared to the normal direction to its surface. This angle noted α will be defined thereafter as the orientation of the tag. In this paper, a method based on incident wave polarization is proposed. The presented approach is able to isolate orthogonal modes of resonance from the measurement and to detect 100% of the useful signal for the detection while keeping a low environment response. In addition, it does not require any knowledge about the tag orientation. This method can be applied to different resonators but loop resonators which are resonators commonly used in chipless RFID [9] are considered in this paper. Indeed, these scatterers can exhibit a strong parasitic mode of resonance and so are a good example for such approach. This work will show how the polarization filtering can remove this parasitic mode

for identification application.

In Section II, the method based on polarization is presented when the EM wave falls upon the tag's surface at normal incidence. Sections III and IV propose simulations and measurements respectively to validate the method. Sections V and VI focus on measurement in real life applications with highly reflective environment and a study of the impact of the distance. Section VII and VIII generalize the approach to non-normal incidence and other resonator topologies. Finally, Section IX concludes the paper.

II. Theory

The loop resonator illustrated in Fig. 1-a is a resonator commonly used in chipless RFID. In this study, the resonator is a metal loop with no substrate. The thickness of the metal is sufficient to give good rigidity to the structure which allows it to be handled and used on different substrates. These loops are widely used in RFID chipless systems because they have no ground plane (only one metal layer) and their geometry allows them to have a high quality factor (above 120 for frequencies around 3 GHz), which is comparable to many ground plane resonators. However, their main disadvantage is that these scatterers have to be read in co-polarization with a precise orientation with respect to the reader's antenna. This orientation related to the α angle shown in Fig. 2. Indeed, the preferred direction is when the incident field is perpendicular to the length of the loop (see Fig. 2 when α=0). The identification of the loop will be possible in this configuration with at least a misalignment of a few degrees. When the loop is illuminated by an incoming electromagnetic field, the maximum energy backscattered occurs at its resonant frequency f defined by [20]:

$$f = \frac{c}{2\sqrt{\varepsilon_{eff}}(l + 2\Delta l)} = \frac{c}{2\sqrt{\varepsilon_{eff}}L} \quad (1)$$

where c is the speed of light in vacuum, ε_{eff} is the effective permittivity seen by the loop, l is the length of the coplanar strip (which corresponds here to the notch's length) and Δl is the additional length taking into account the presence of non ideal short circuit (SC) discontinuities as illustrated in Fig. 1-b. It is clear from Fig. 1-b that the loop resonator can be considered as a transmission line section terminated at both ends by SCs [20]. This additional length can be obtained through simulations or by measurement [20]. Note that, the effective length $L = l + 2\Delta l$ will be used in the following parts of the paper.

To improve the robustness reading of this resonator, it is important to notice that depending on the incident E-field orientation this resonator can present two modes of resonance: a dipole-like mode A_d and a loop-like mode A_l. So, in the general case (when the tag is positioned in any way in relation to the antenna), both modes can be excited and the total measured radiated field will be the complex summation of the two. To show this, the loop resonator with the dimensions given in Fig. 1-a is simulated using CST MW and the transient solver. The resonator is first oriented at 40° to the incoming electric field. Simulation results are plotted in Fig. 2. A wide peak can be seen at 2.5 GHz corresponding to the dipole mode

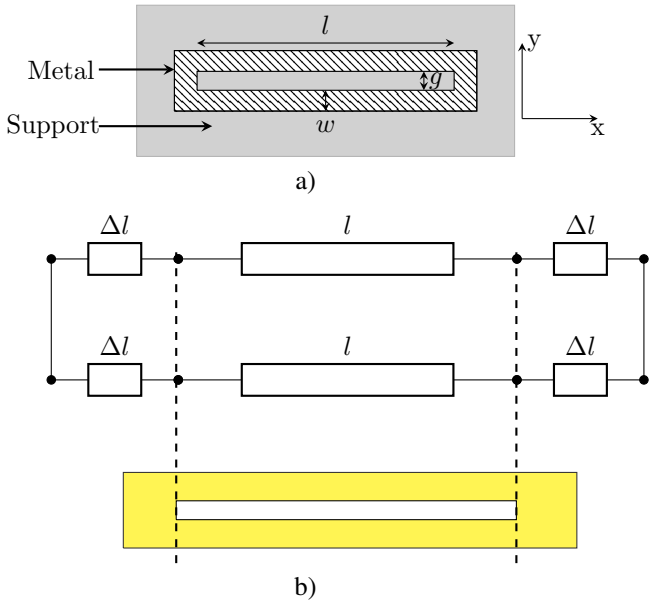

Fig. 1. (a) Nominal dimensions used for the fabrication: l=50.83mm , g=2.07mm and w=1.43mm. (b) Equivalent transmission line model of a loop resonator [20].

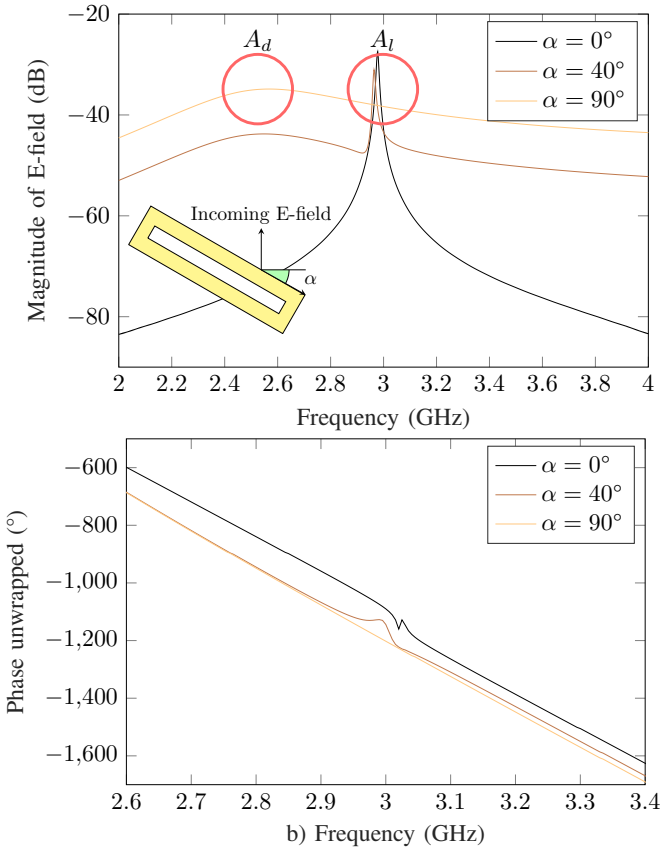

Fig. 2. a) Simulated E-farfields corresponding to S_{11} parameter of a loop for different values of α in amplitude and b) in phase. The incoming E-field according to the resonator is shown in Fig. 2. The angle α goes from 0° to 90° with 10° steps.

A_d and a sharper peak at 3 GHz from the loop mode A_l. We will see that polarization filtering introduced here will permit

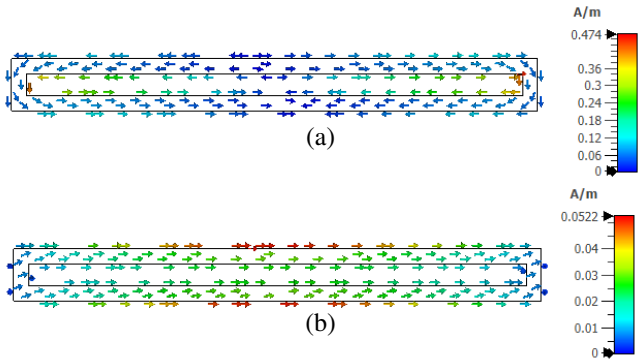

Fig. 3. (a) Current distribution on the loop resonator for the loop mode A_l at 3GHz and (b) the dipole mode A_d at 2.5GHz.

to remove the parasitic mode to facilitate the extraction of the information contained in the tag, whatever its orientation in relation to the reader. It can also be seen that for $\alpha = 0°$ the tag is easily detectable (only the resonance mode A_l linked to the identifier is present) and for $\alpha = 90°$ it is not possible to catch the resonance frequency. The further away from the condition $\alpha = 0°$ the more difficult the reading, which shows a significant limitation.

It has been shown in [33] that the loop mode A_l scattering phenomenon is associated to the induced current on the extremities of the resonator. This phenomenon can be confirmed by the simulated current distribution at the resonance of the loop mode (see Fig. 3-a).

To describe this specific mode of resonance A_l, the loop resonator can then be modeled as two infinitesimal dipoles spaced by $\lambda/2$ and backscattering a wave in phase. This equivalence is illustrated in Fig. 4-a. Indeed, when we send a wave in the direction of the loop at the resonance frequency of the scatterer, the collinear part of the wave with respect to the orientation of the dipole will exist the fundamental mode of this structure. As described on Fig. 3-a, this mode makes appear a current in phase on both ends of the loop (the current present on the long sides of the rectangular loop does not produce any radiation because of the observed symmetry). This is why the field backscattered by the loop behaves like the field created by two infinitesimal dipoles positioned at the two ends of the scatterer, and existed in phase. From an analytical point of view, this backscattered field E_{bs} can be obtained by considering the expression of the field radiated by an infinitesimal dipole to which we apply the array factor to describe the two radiating elements. The expression thus obtained is as follows:

$$E_{bs} = k\frac{\eta I_0 L}{16\pi r}\sin(\theta)\frac{\sin\left(\pi\sin(\theta)\cos(\phi)\right)}{\sin\left(\frac{\pi}{2}\sin(\theta)\cos(\phi)\right)} \tag{2}$$

where k is the wavenumber, η impedance of free space, I_0 the uniform current flowing through each dipole with length L and r is the distance between the center of the coordinate system (loop center) and the observation point of the E-field also defined by θ, ϕ. For this resonance mode, the radiation pattern but also the polarization of the backscattered wave can be determined using (2). Note that the Q-factor associated to this mode is high as seen by the sharp peak in the S-parameters (see Fig. 2). Due to its sharpness, this mode is the one wanted in chipless RFID when using loop resonators for identification or sensing applications [33].

The second mode of excitation is when the currents are induced on the whole resonator as shown in Fig. 3-b. The scattering mechanism is closer to a single short circuited dipole (without ground plane) as illustrated by its equivalent model in Fig. 4-b. Here, the radiation pattern but also the polarization of the backscattered wave by a dipole are known in the literature [34]. It should be noted that the two resonance frequencies are very close to each other (relative to distances l and $l + 2w$ respectively) and cannot be suppressed simply by design or even with time gating. Thus, as illustrated in Fig. 4, the two modes of resonance of the loop resonator can be associated to dipoles which are orthogonal to each other. This orthogonality can be used with a polarization filtering approach as discussed below to extract the parasitic mode of resonance. Indeed, by filtering the two modes using the polarization of the backscattered wave, the parasitic signal can be removed but also the peak prominence is improved.

We will also see that the method proposed here is not limited to the suppression of the dipole mode of the loop, but in a more general way will allow to subtract all the reflections coming from the environment which are 1) excited by the incident wave (direction of port 1) and 2) whose polarization of the backscattered signal is aligned with the direction of the dipole A_d. This is why the interest of this method is not limited to the dipole resonator (even if it is a very good example because of the presence of the dipole mode) but applies whatever the scatterer. The demonstration will be done considering that the environment reflects a wave in the direction of the Ed dipole and we will treat in Section VIII, the case of a completely different resonator (resonator with ground plane) for which the method will also apply with a notable gain on the robustness of reading. Unlike a cross-polarization measurement, we will see that this method does not reduce the influence of the environment in the A_l direction (Section VII). However, without this property, we will see that it is possible to apply this method with a notable improvement in the read distance even when the tag without ground plane is in the presence of a large reflecting object (Section V) as well as for tags with ground plane (Section VII, where time gating can be combined with the proposed approaches to deal with this issue).

A dual-polarization antenna (2-ports) will be used for the study. The coordinate system and the preferred directions to excite the loop modes are illustrated in Fig. 5. When the resonator is rotated by the angle α, the polarization scattering matrix S (Sinclair matrix) which relates the scattered electric field vector E_s to the incident field vector E_i is [35] :

$$S(\alpha) = \Omega \times S(0°) \times \Omega^T \tag{3}$$

with

$$S(0°) = \begin{pmatrix} A_l & 0 \\ 0 & A_d \end{pmatrix}, \quad \Omega = \begin{pmatrix} \cos\alpha & \sin\alpha \\ -\sin\alpha & \cos\alpha \end{pmatrix} \tag{4}$$

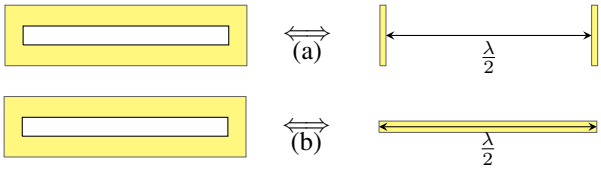

Fig. 4. (a) Equivalent model of the loop resonance for the A_l mode. The loop is modeled by two infinitesimal short circuited dipoles spaced by $\lambda/2$ with $\lambda/2$ corresponding to the notch l length. (b) Equivalent model of the dipole resonance for the A_d mode. The loop is modeled by one short circuited dipole of length $\lambda/2$ with $\lambda/2$ corresponding to the total length of the resonator $l + 2w$.

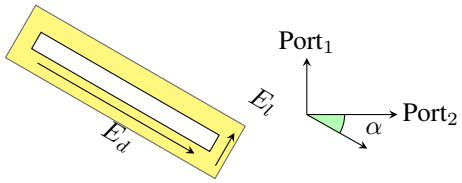

Fig. 5. Coordinate system considered in the paper. Port$_1$ and Port$_2$ are the ports of the dual-polarization horn antenna. The rotation α is between the Port$_2$ and the direction of A_d.

and T denotes the transpose. As previously explained, the coefficients of the scattering matrix S, A_n denotes the contribution of the resonance in the direction of mode E_n. S-parameters coefficients for the angle α can there be written :

$$\begin{cases} S_{11}(\alpha) = \sin(\alpha)^2 A_d + \cos(\alpha)^2 A_l + E_{11} \\ S_{21}(\alpha) = \sin(\alpha)\cos(\alpha) A_d - \sin(\alpha)\cos(\alpha) A_l + E_{21} \end{cases} \quad (5)$$

where E_{xy} corresponds to the environment response (without the loop) in the direction of the $xy-$port of the antenna. So both modes are given by :

$$\begin{cases} A_l = [S_{11}(\alpha) - E_{11}] - \tan(\alpha)\,[S_{21}(\alpha) - E_{21}] \\ A_d = [S_{11}(\alpha) - E_{11}] + \cot(\alpha)\,[S_{21}(\alpha) - E_{21}] \end{cases}. \quad (6)$$

An initial measurement without the resonator is done to get E_{11} and E_{21} and then the tag is placed. If the rotation angle of the loop α is known as well as $S_{11}(\alpha)$ and $S_{21}(\alpha)$, (6) can be used directly to extract only A_l (and so the tag ID), removing the parasitic mode A_d. If the rotation of the loop α is unknown, a numerical resolution can be done in order to estimate this angle. More information about this resolution can be found in section III. This second approach allows to correctly apply the presented method as well as to add a rotation sensor capability to the existing identification functionality of the chipless RFID tag. Notice that this approach can be used to improve the readability of a loop resonator without indication of its position but also as an orientation sensor following the first remark. This ability to read a tag regardless of its orientation is also a way to improve reading robustness in real applications [29].

Notice that for α=0° or α=90°, (5a) or (5b) does not grant solutions. Indeed, for these values the mode is not excited or not received (orthogonal to the antenna ports) hence this result. It is possible however to use S_{22} and S_{21} in such cases to remove this problem since these ports are orthogonal to S_{11} and S_{12}, they will excite and receive the modes.

It is clear from the second part of (6) that this method suppresses the dipole mode of the loop A_d but also the contribution of the environment which is aligned with the direction of the loop A_d. Previously, we have considered the term A_d as the dipole mode of the loop resonator. However, in a more general case, A_d represents the total contribution of the backscattered field perpendicular to the preferred reading direction (E_l) of the tag by the rotating target, a target consisting of the tag and any support that would rotate or not with the tag. Indeed in this term A_d, we can take into account both the presence of a parasitic mode (example specific to the loop), or the quasi-optical mode of the tag or the contribution of the support on which the tag is attached (we have chosen to illustrate the method on a loop insofar as with this parasitic mode, this structure alone has a significant contribution in this specific direction E_d). Like the parasitic mode of the loop, depending on the angle of this target in relation to the reading antenna, A_l is directly involved in the measured signals S_{11} and S_{21} [see (5)] and therefore negatively impacts the tag reading by adding to the signal a contribution not including the ID of the tag which necessarily reduces the ratio between the useful signal and the total signal measured and thus results in the end in a reduction of the reading distance. Thus, as we will see in practice, this possibility to remove a part of the environment which does not include useful information on the tag will allow a significant increase in the reading distance. A practical case study will be discussed in section IV. We note, however, that this approach does not overcome the unknown contribution of the environment or the quasi-optical mode of the tag in the preferred reading direction (E_l). This is for example the case when a large metal plate is positioned behind the loop (see section V) or when tags with a ground plane are used. Since these two configurations are commonly used in practice, in section V and VIII a modified version of the approach introduced here will be applied. It will be shown through these examples that the approach is general and allows a reading improvement for any chipless tag based on the use of resonators, with or without ground plane and this in different environments.

Last but not least, 100% of the useful signal of A_l is captured using (6) whereas only 1/4 is captured when only measuring S_{21} with a tag at 45° as it is done today hence improving the SNR and so the maximum reading range.

III. Angle Estimation

Let's consider the loop resonator of Fig.5. The polarization axis of A_l is along the E_l axis. If the antenna polarization port 1 matches the A_l axis, 100% of the resonance is received on port 1 and 0% on port 2. Now, if the resonator is rotated at 45°, 50% is received on port 1 and 50% on port 2. So, if we tell that 100% on the resonator is received on 1 port and 0% on the other port, we know that the coordinates system of Port1/Port2 is aligned with the resonator. We are using this principle to estimate the angle rotation α.

Using (6), we have a rotating coordinate axis. If we rotate the coordinate system to match the A_l axis, port 1 of the coordinate system has 100% of the power while port 2 of the

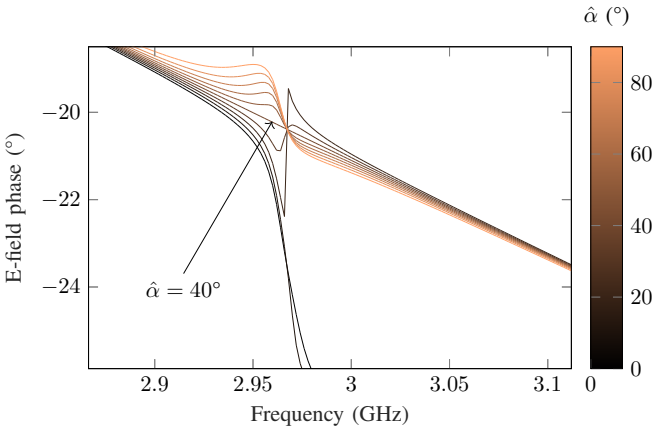

Fig. 6. Unwrapped phase of the dipole mode A_d computed with (6) when the resonator is oriented at $\alpha = 40°$ for different values of estimated $\hat{\alpha}$.

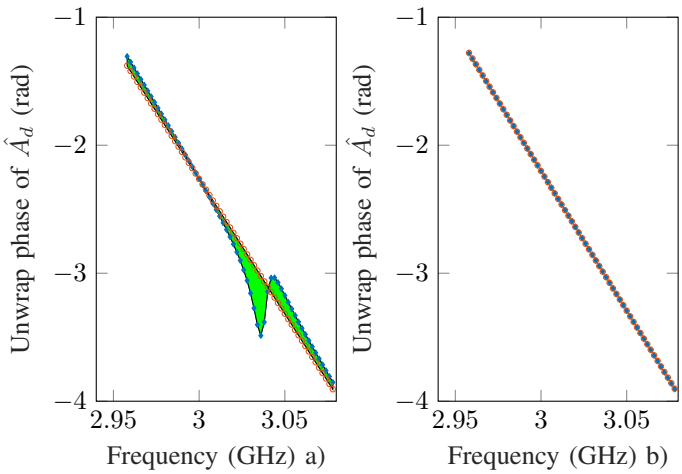

Fig. 7. Phase of $\hat{A_d}$ in blue (square markers) and its linear fit in red (circle marks) for a) $\hat{\alpha} = 35°$ and b) $\hat{\alpha} = 45°$ for a simulated loop in CST MW with $\alpha = 45°$. The green surface represents the difference between the phase and the fitting.

rotating axis has 0%. To estimate if no signal is received on port 2, we can look at the phase at resonance of A_l. Indeed, at resonance, a jump on the phase is present due to the resonant behavior (see Fig. 6). Hence to estimate the rotation of the resonator, the following algorithm is implemented in Matlab :

```
1  [S11,F] =extract('S11.txt','re_im');
2  S21=extract('S21.txt','re_im');
3
4  best_alpha=zeros;
5  best_norm=1e9;
6
7  for alpha=-180:1:180
8      Ad= S11 + cotd(alpha)*S21;
9
10     [¬,S]=polyfit(F, unwrap(angle(Ad)),1);
11     if(S.normr < best_norm)
12         best_norm=S.normr;
13         best_alpha(ID) = alpha;
14     end
15 end
16 disp(['Estimated alpha :' num2str(best_alpha)])
```

Listing 1. Matlab implementation to estimate α.

The numerical resolution tries all the angles from -180° to 180° until port 2 no longer has a phase jump at the A_l resonance: so the rotating axis port 1 is aligned with the resonator. The value of $\hat{\alpha}$ which gives no phase jump is the one with the lowest norm of the residuals of a fitting with linear function (line 10 of the algorithm). An illustration is given in Fig. 7 where a loop resonator is simulated at $\alpha = 45°$. The phase of $\hat{A_d}$ for $\hat{\alpha} = 35°$ and $\hat{\alpha} = 45°$ are presented with their respective linear fitting. Since the loop is placed at $\alpha = 45°$ and A_d is orthogonal with A_l, no phase jump due to resonance is present for $\hat{\alpha} = 45°$ on the phase of $\hat{A}_d$.

IV. Simulations

Simulations have been carried out using CST MW to validate the proposed approach. A plane wave excitation along the direction noted Port_1 in Fig. 5 was used. The loop dimensions for the simulation part but also for the loop used in measurements are shown in Fig. 1. E-farfield probes at 1meter from the loop, relating to the directions Port_1 and Port_2 in Fig. 5, and thus corresponding to S_{11} and S_{21} parameters have been extracted when the tag rotates as illustrated in Fig. 5. These two quantities are plotted in Fig. 2a and Fig. 8 respectively. At $\alpha = 0°$, only the A_l mode can be excited and received by Port_1, as demonstrated in Fig. 2a. At $\alpha = 90°$, only the A_d mode can be excited and received by Port_1; this is also confirmed in Fig. 2a. Between $\alpha = 0°$ and $\alpha = 90°$, both modes are excited and a contribution of each is seen in the simulations. For the S_{21} parameter, excited modes cannot be received at $\alpha = 0°$ or $\alpha = 90°$ due to the position of the loop regarding to the incident wave and the received probe. For this reason simulated E-fields corresponding to S_{21} have not been plotted in Fig. 8. Between $\alpha = 0°$ and $\alpha = 90°$, the contribution of the two modes follows (5). So, by applying (6), the modes A_d and A_l can be isolated from each other. The mode that includes the tag ID (A_l) is plotted in Fig. 9. By removing the dipole mode contribution, the loop mode can be found perfectly. It is also clear that the extracted curve is rotation independent (as long as α is correctly estimated as it is the case in Fig. 9). The dipole mode A_d is plotted in Fig. 10 as an example. The dipole mode is clearly found, with some residual contributions of the loop mode around its resonance frequency due to numerical errors. The simulations are in good agreement with the theory, namely that it confirms the orthogonality of the two modes and therefore the possibility of separating them.

Fig. 6 illustrates the resolution approach to estimate the value of α. The unwrapped phase of A_d is plotted versus frequency for several values of estimated $\hat{\alpha}$. By varying $\hat{\alpha}$, the criterion $\alpha = \hat{\alpha}$ is verified when the loop mode and dipole mode are independent from each other, i.e. when the A_d mode obtained after projection (6) is independent of the loop mode and therefore only the contribution of the dipole mode is present. For this reason, by looking at the phase of A_d, we know that the loop mode is not present if no non-regular variation of the phase around the resonance frequency of the loop mode is present. A numerical resolution consists

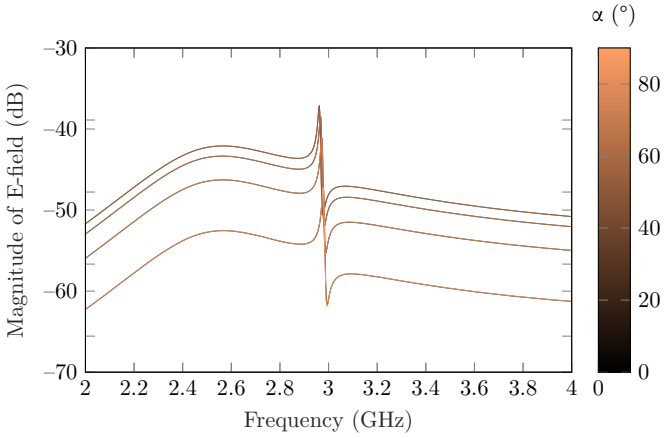

Fig. 8. Simulated E-farfields corresponding to S_{21} parameter of a loop for different values of α. The incoming E-field according to the resonator is shown in Fig. 2. The angle α goes from 0° to 90° with 10° steps.

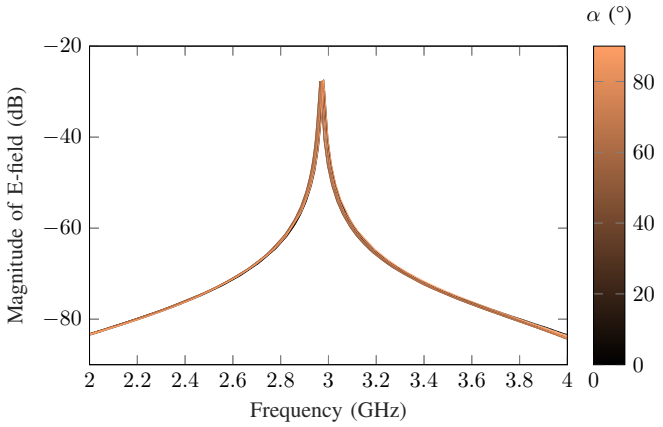

Fig. 9. Extracted loop mode A_l using (6) for different values of α.

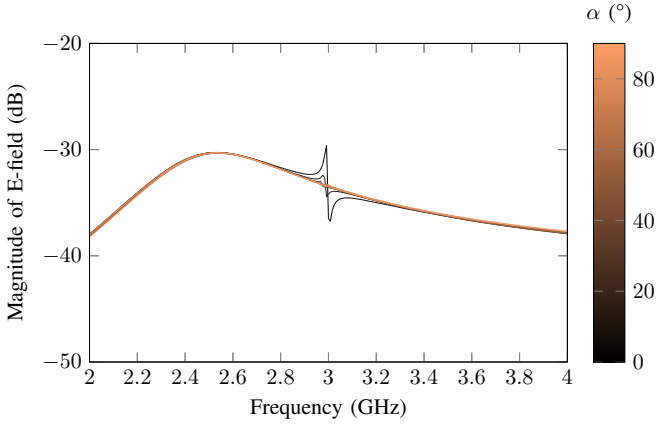

Fig. 10. Extracted loop mode A_d using (6) for different values of α.

of linear fitting the phase A_d near the A_l resonant frequency. The correct value of $\hat{\alpha}$ is the one that minimizes the norm of the residues of the linear fitting. In Fig. 6 the loop resonator is placed with $\alpha = 40°$ and the only value of $\hat{\alpha}$ that presents no phase variation on the estimated A_d is $\hat{\alpha} = 40°$.

In general, the direction perpendicular to the loop axis, in addition to admitting the dipole resonance mode A_d, can also recover a parasitic field contribution reflected from the environment. This contribution negatively impacts the detection system. We can see that (6) allows to reduce this contribution, that can be considered as external noise. The reduction of these environment responses is not visible in the simulation since this effect is not taken into account in the simulator. However this significant effect will be seen in section V and VI on measurements in real environments.

For comparison with the introduced approach, time-gating (TG) technique will be applied to the loop resonator at $\alpha = 45°$. In Fig. 11, the frequency response (backscattererd E-fields obtained from a probe on CST with plane wave excitation, i.e. quantities similar in measurement to the parameters S_{11} and S_{21}) of the simulated loop is presented along the extracted modes A_d and A_l. We can see that the mode of interest A_l is correctly extracted. If we look at the time domain representation of the E-fields in Fig. 12, we can see that it is difficult without any post processing to differentiate the differents modes in the response. Now if we apply (6) on these time signals, we can compute the time response of each mode as illustrated in Fig. 13.

The mode A_l is resonating for a longer time than the mode A_d due to its higher Q-factor. From Fig. 13, to remove the response of A_d from the signal, a time-gating with a $t_{start} = 7$ns is needed. With such t_{start}, time-gated signals TG S_{11} and TG S_{21} are presented in Fig. 14. We can see that the A_l mode present in TG S_{11} and TG S_{21} is also partly removed hence the peak apexes of these two curves have lower amplitudes. Indeed, the time-gated signal is 8dB lower than the A_l mode. This is because the time-window 7ns on S_{11} or S_{21} also remove A_l's signal as showed in its time response in Fig. 13. Futhermore, as said previously, it is difficult to estimate t_{start}. In practice, to limit the effect of the present of the object on which the tag is fixed, one can choose to cut off the order of 1ns from the maximum of the time response signal (which here makes $t_{start} = 4.5$ns, see Fig. 13). In this case, the result that we would have is presented in Fig. 15. We can see that the time-gated signals are not as pure as the A_l signal. The problem in this case is that if for a given ID, another scatterer could resonate around 2.4 GHz, it would be impacted by the presence of the A_d mode. The peak amplitude is also lower than the A_l amplitude by 6dB. Since less signal was removed (2.5ns time-window difference), the amplitude difference with A_l is lower. Finally, if we compare the results between Fig. 14 and 15, we can say that the approach introduced here allows us to suppress the entire spurious mode. If we had tried to cut the spurious mode with time-gating (Fig. 14), we would have significantly degraded the useful signal, reducing the signal-to-noise ratio and thus the read range.

In summary, the proposed method allows to improve the reading robustness of the resonant scatterers. This approach can be advantageously used in combination with the time-gating method (see Section VI). It allows to isolate different resonance modes that time-gating can hardly separate.

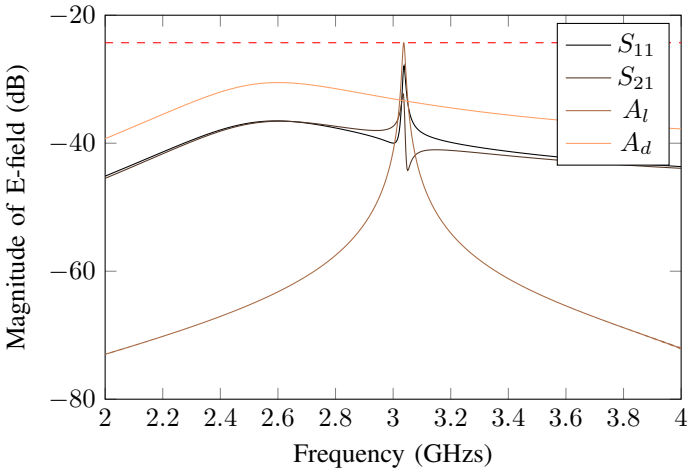

Fig. 11. Frequency response of E-fields corresponding to S-parameters of a simulated loop at $\alpha = 45°$ along with A_d and A_l obtained with (6).

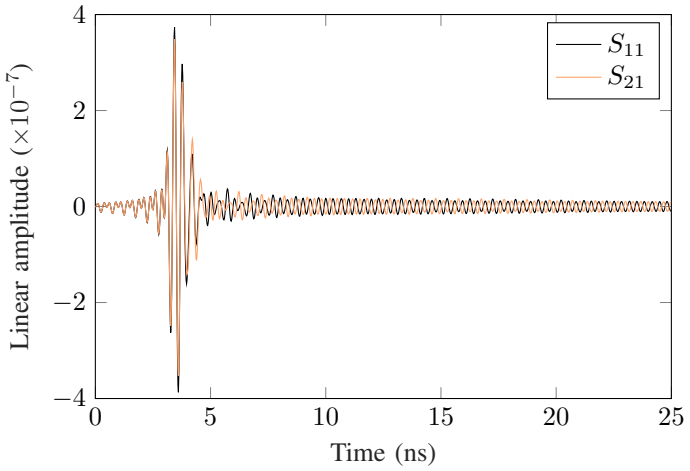

Fig. 12. Time domain representation of E-fields corresponding to S-parameters plotted in Fig. 11 of a simulated loop at $\alpha = 45°$.

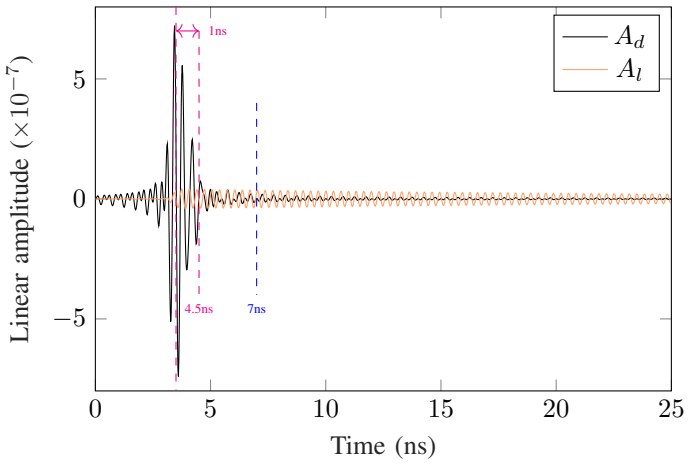

Fig. 13. Time response of A_d and A_l obtained with (6) for a simulated loop at $\alpha = 45°$.

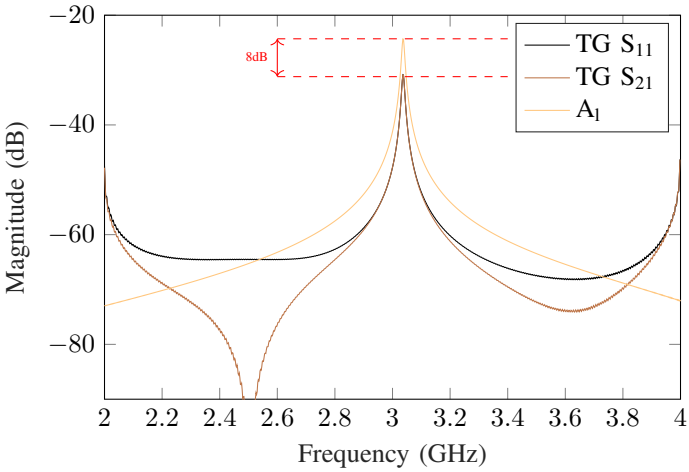

Fig. 14. Comparison of time-gated S-parameters with $t_{start} = 7$ns and A_l obtained with (6).

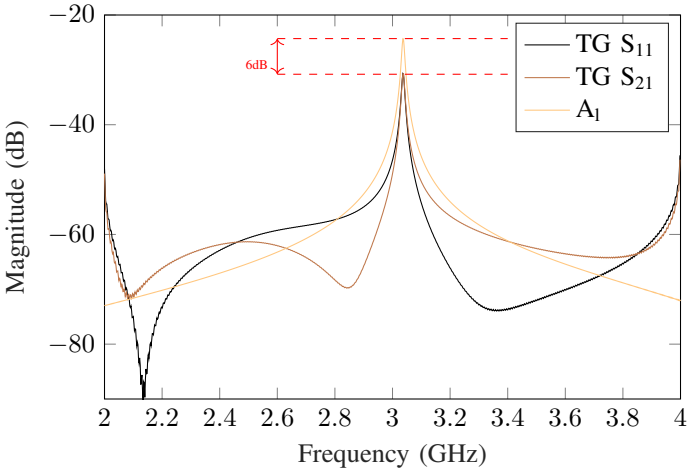

Fig. 15. Comparison of time-gated S-parameters with $t_{start} = 4.5$ns and A_l obtained with (6).

V. Measurements

The test-bench setup is presented in Fig. 16. Experimental measurements are performed using a VNA (Agilent 5222A). The source power of VNA is equal to 0 dBm. The frequency sweep ranging from 2 to 3 GHz with 10001 points is used. A co-polarization bistatic configuration with Satimo (QH2000) quad ridged open boundary antennas (2–32 GHz) is used. The measurements are done in a real environment with people in close proximity. A first measurement is done without the resonator. After that, the resonator is placed in front of the antenna and the first measurement is subtracted to the new measurements to remove the response of the environment. The loop resonator can rotate for different values of α ($\alpha = 0$ corresponds to the direction of Port 1). A spacer in polystyrene of 5 cm is used to separate the resonator from the antenna. A protractor is placed under the loop to measure α as the resonator rotates. S_{11} and S_{21} measurements are done and plotted in Fig. 17 and Fig. 18 respectively. S_{11} is in good agreement with the simulation, but S_{21} presents a dip instead of a peak at the resonance frequency. This is due to a

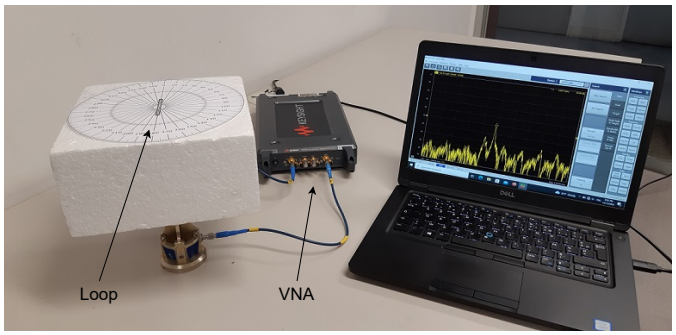

Fig. 16. Measurement setup.

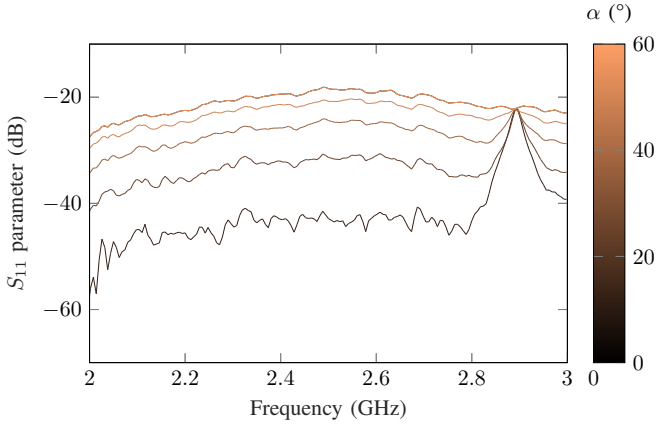

Fig. 17. Measured $|S_{11}|$ parameter of the loop for different rotation angles α.

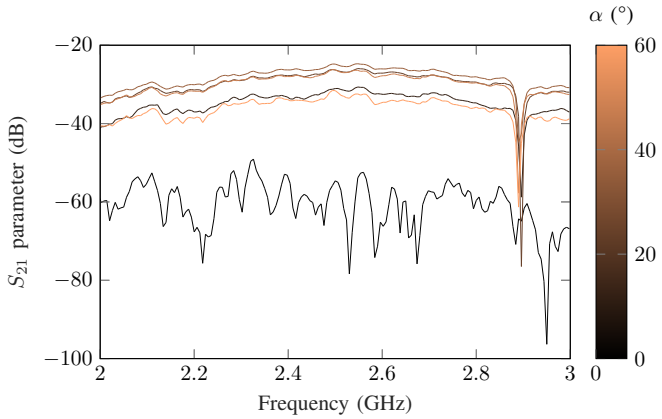

Fig. 18. Measured $|S_{21}|$ parameter of the loop for different rotation angles α.

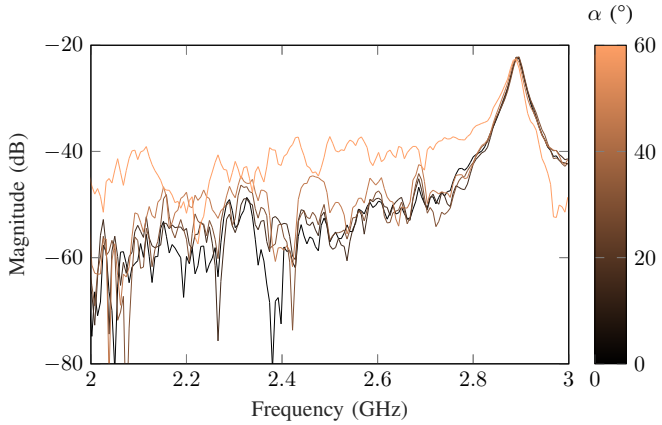

Fig. 19. Extracted loop mode A_l (magnitude) for different rotation angles α using (6) and the estimated $\hat{\alpha}$.

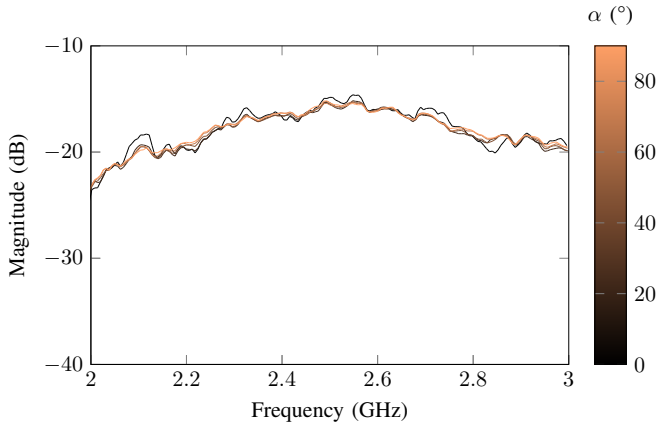

Fig. 20. Extracted dipole mode A_d (magnitude) for different rotation angles α using (6) and the estimated $\hat{\alpha}$.

phase opposition between the resonator contribution and the environment (not considered in simulation). With these S-parameters and the dipole mode A_d phase, α is estimated as previously explained. The angle value α measured with the protractor can be compared with the estimated $\hat{\alpha}$ and both values are listed in Table I. The estimated and real angle values are in good agreement with a maximum difference of 5°. This shows that the method can also be used to determine the angle of the loop to the antenna. When α is found, (6) is used to extract the loop mode A_l which is plotted in Fig. 19. Like in simulation (Fig. 9), we can see that the peak is more visible when (6) is applied but also that the peak does not change with α. The noise is higher for the measurement at $\alpha = 60°$ which is also the measurement where the guessed $\hat{\alpha}$ have the highest error of 5°. The dipole mode A_d is plotted in Fig. 20 for illustration.

When a chipless RFID tag is composed of several loop resonators, the technique is still valid; it is even more efficient because the dipole mode of each loop can impact a loop mode of another loop. Also the possibility to remove it will increase the peaks prominence of each scatterer. This idea is presented in Fig. 21 where a tag of 4 loop resonators is placed at $\alpha = 45°$. The raw measurement where the environment is subtracted with a first measurement gives the S_{11} parameters in orange where prominence of each resonator peak is quite low. Equation (6) is applied resulting in the improved ratio between the amplitude of loop modes and noise. The residual environment as defined in [36] is reduced by -12dB in minimum.

VI. Impact of Highly Reflective Environment

In this section, we want to emphasize the improvement of the reading robustness of this approach according to the environment. As explained in Section II, the introduced method

TABLE I
REAL ANGLE α AND ESTIMATED ANGLE $\hat{\alpha}$ USING THE PHASE OF A_d.

Real angle α	0°	15°	30°	45°	60°
Estimated angle $\hat{\alpha}$	0°	14°	30°	45°	65°

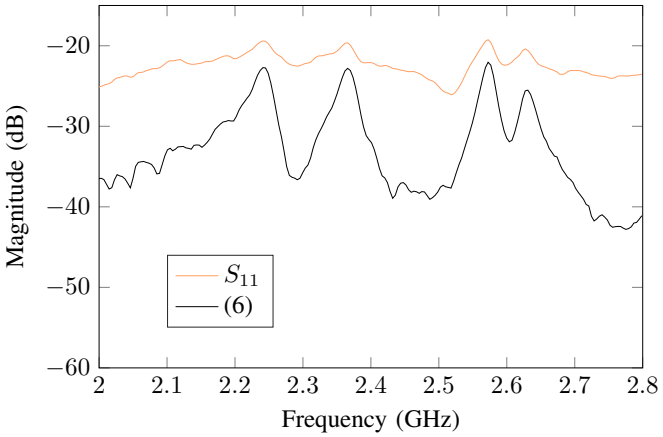

Fig. 21. Comparison of the S_{11} measurement and the post-processing done with (6) on a tag composed of 4 loop resonators placed at 45°.

eliminates the total contribution of the environment and the tag oriented perpendicular to the preferred reading direction (E_l). The measurement setup in this highly reflective environment is illustrated in Fig. 22. A metallic plane is placed below the loop resonator to increase the reflection of the incoming electromagnetic wave, introducing a higher residual environment. A spacer of polystyrene is used to reduce the coupling effect between the loop and the metallic plane that would change the scatterer resonant frequency. The measured S-parameters of this configuration are presented in Fig. 23 when the resonator is placed at 45°. Raw S-parameters and S-parameters with background subtraction (the background measurements noted E_{11} and E_{21} in (6) are done with the metallic plate) are compared in Fig. 23. Note that the presence of the resonance is hardly visible for S_{11} and S_{21} with background subtraction . Indeed, S_{11} with background subtraction presents a very weak peak, while S_{21} with background subtraction presents a dip due to the dipole mode very present for this orientation of the tag. When (6) is applied to the S-parameters with background subtraction, the resonance frequency is easily observable with a peak prominence of 10dB. Time-Gating (TG) post processing is used for comparison with optimised $t_{start} = 3$ µs and $t_{stop} = 3.1973$ µs. Results are presented in Fig. 24. We can notice that (6) gives a better peak prominence than TG (10dB higher) because it is able to use 100% of the resonator useful signal (6dB) and it also compensates for the resonator misorientation (4dB). Measurements have been achieved for different apriori unknown orientation angles α of the resonator in front of the metallic plane. Extracted A_l modes using (6) are plotted in Fig. 25. We can see that the residual environment is always reduced while the resonator amplitude remains constant when the resonator rotates since the total energy is conserved during the post processing.

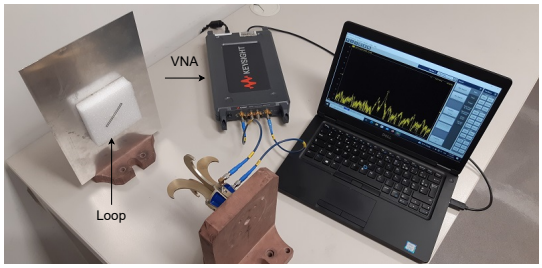

Fig. 22. Measurement setup used to measure a loop resonator on a highly reflective support.

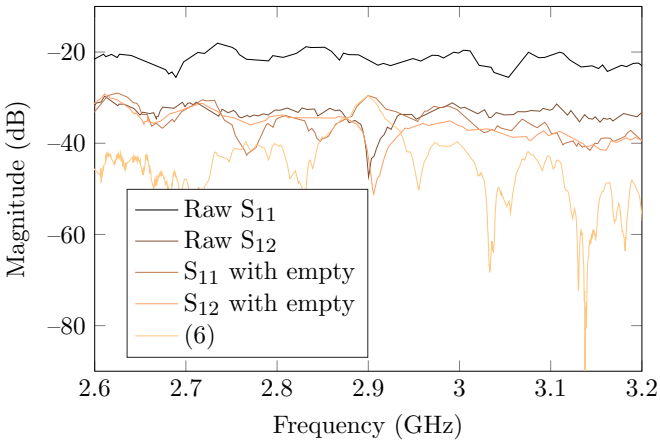

Fig. 23. Measured S_{11} and S_{21} of the loop resonator at 45° in front of a metallic plane (see Fig. 22) compared with the use of (6).

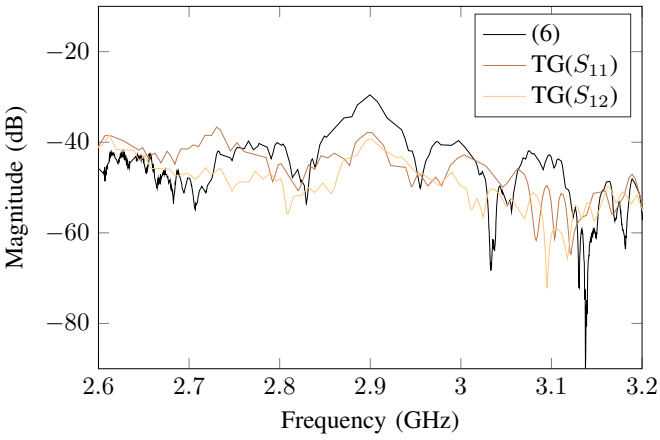

Fig. 24. Extracted loop mode A_l of the loop resonator at 45° in front of a metallic plane (see Fig. 22) with (6) compared with the time-gating (TG) method. Angles are not apriori known.

VII. IMPACT OF THE DISTANCE

A study of the readable distance of a chipless tag (loop on Rogers RO4003C with $\varepsilon = 3.55$) has been done. The test bench used for this measurement is illustrated in Fig. 26. The resonator is placed on a polystyrene support ($\varepsilon \simeq 1$) above the antenna. S-parameters are measured and then the distance between the antenna and the tag is increased from $d = 1.5$cm to 84.5cm by adding a new polystyrene support. For each distance, S_{11} and S_{21} raw measurements are compared with the proposed approach (6) as well as with the S_{11} and S_{21}

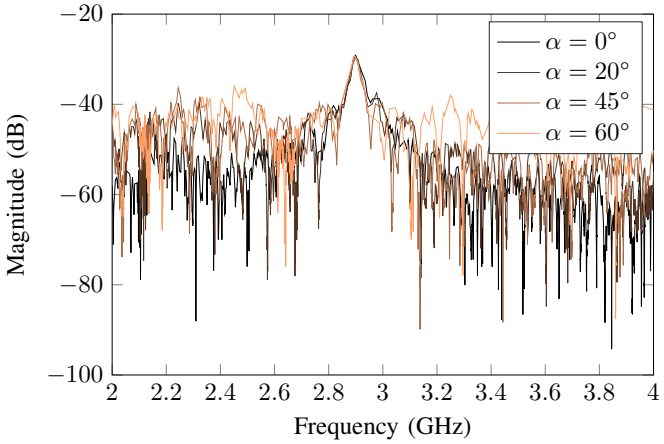

Fig. 25. Extracted mode A_l of the loop resonator for different angles α in front of a metallic plane (see Fig. 22) with (6).

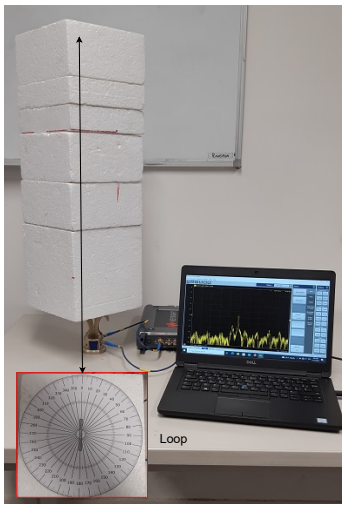

Fig. 26. Measurement setup used to study the readable distance of the resonator.

parameters where TG is applied. For each distance, TG parameters' (t_{start} and t_{stop}) are deduced from the inverse Fourier transform of the S-parameters to maximize the accuracy of the response.

The loop resonator is placed at $\alpha = 45°$. Comparisons for distances $d = 1.5$ cm and $d = 20.5$ cm are plotted as examples in Fig. 27 and Fig. 28 respectively. A quantitative criterion was chosen to consider if a loop resonator can be read or not. The criteria are the following : the peak prominence should be +10dB or higher, the maximum amplitude in a frequency span of 0.15 GHz must be greater than -50dB (this must correspond to the amplitude of the resonance peak). This procedure is done using the *findpeak* function in Matlab. Results are presented in Table II where a "1" indicates that the peak is detected and a "0" when it is not, considering these criteria. We can see that for a loop resonator placed at 45°, these criteria are never valid for raw measurements of S_{11} and S_{21} because the +10dB peak criterion cannot be met due to the presence of the A_d mode and the environment response. With the TG technique, it is possible to satisfy correctly this criterion up to 64,5 cm. After that, the signal amplitude goes below the -50dB threshold and the peak predominance of +10dB with the environment noise is not respected. The limitation of the TG approach is due to the fact that some part of the useful signal will be removed hence deteriorating the peak signal. On the contrary, the idea introduced here is that when doing the projection with (6), we are retrieving 100% of the useful signal while reducing other parasitic signals, hence keeping a better peak prominence. By using (6), the peak is better marked as shown in Fig. 27 and Fig. 28 allowing an increase of 30 cm compared to the TG on a readability with a maximum distance of 84,5 cm.

The tag is now composed of 4 resonators and is measured as a function of distance. The same tag configuration as the one presented in Fig. 21 is used. The same criteria as previously described are used with a frequency span of 0.65GHz for resonators between 2.2 GHz and 2.7 GHz (see Fig. 21).The number of peaks correctly detected up to 4 are plotted in Table III. We can see that raw S_{11} and S_{21} never succeed to respect these criteria for the 4 resonant frequencies. Since the tag is now composed of 4 resonators, the post-processing to implement the TG approach is harder

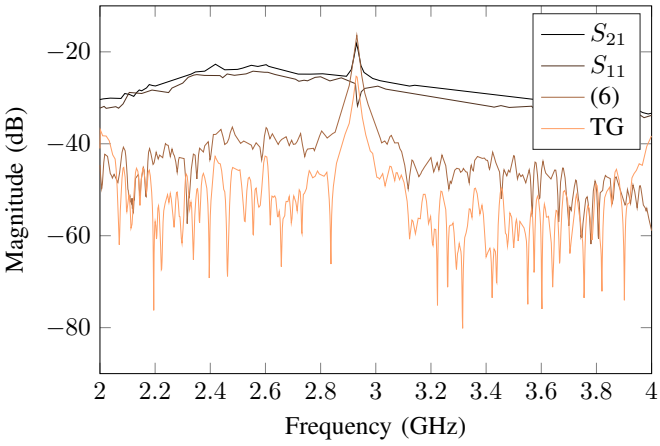

Fig. 27. Raw S-parameters and post-processed S-parameters [with (6) and TG] for a distance between the resonator and the antenna of *d*=1.5 cm.

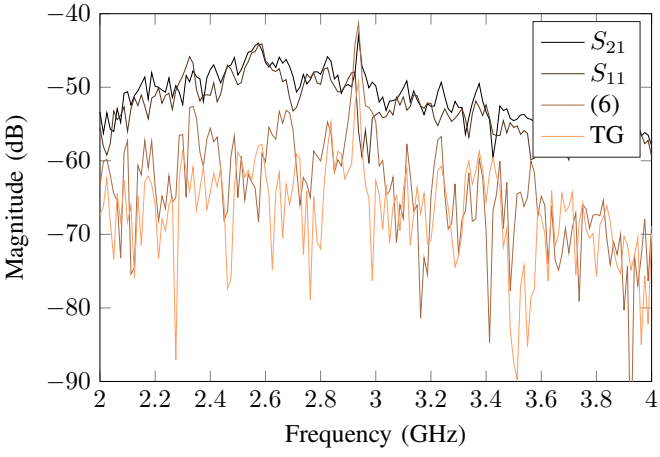

Fig. 28. Raw S-parameters and post-processed S-parameters [with (6) and TG] for a distance between the resonator and the antenna of *d*=20.5 cm.

TABLE II
RESEARCH OF THE PEAK RESONANCE (PROMINENCE OF +10DB ON A FREQUENCY SPAN OF 0.15GHZ AROUND THE RESONANCE FREQUENCY AND ABOVE -50DB OF AMPLITUDE).

Distance (cm)	S_{11}	S_{21}	(6)	Time-Gating
1.5	0	0	1	1
13.5	0	0	1	1
20.5	0	0	1	1
27.5	0	0	1	1
39.5	0	0	1	1
44.5	0	0	1	1
49.5	0	0	1	1
54.5	0	0	1	1
59.5	0	0	1	0
64.5	0	1	1	1
74.5	1	1	1	0
79.5	0	0	1	0
84.5	1	0	1	0

TABLE III
NUMBER OF PEAKS DETECTED OF +10DB ON A FREQUENCY SPAN OF 0.65GHZ AND ABOVE -50DB OF AMPLITUDE.

Distance (cm)	S_{11}	S_{21}	(6)	Time-Gating
3	1	1	4	4
13	1	1	4	2
23	0	0	4	2
34	0	2	4	2
44	0	1	3	0

since higher resonant frequencies tend to attenuate sooner in time than lower frequencies. Choosing a lower t_{start} allows to capture more high frequency signals but also environment noise. For these reasons, the TG method is not able to respect the imposed criterion as soon as the distance is higher than 13 cm. However, the proposed approach allows to see the 4 peaks up to 34 cm. Notice that reading distance decreases because the tag composed of 4 resonators has resonators with a lower Q-factor than the resonator used alone (see Table II).

VIII. CASE OF AN ANTENNA NOT PLACED IN NORMAL INCIDENCE WITH RESPECT TO THE TAG

In the previous cases, the loop resonator is rotated in the xOy plane and the antenna is placed in a plane parallel to the xOy plane. In a more general case, the antenna is aiming at the resonator not necessarily in a parallel plane. In this case, a spherical coordinate system can be attached to the loop to indicate the position of the antenna as illustrated in Fig. 29. The resonator is placed in the xOz plane and rotates around the $\vec{y}$ direction with an angle α_y. As in section III, this α_y angle corresponds to a rotation with respect to the normal of the plane in which the tag is positioned. The antenna is directed towards the tag and its position in space is given by the angles θ and ϕ. As before, the position of the antenna relative to the tag (i.e. θ and ϕ) is assumed to be known. The dual-port antenna will sense the fields along the axis $\vec{\theta}$ and $\vec{\phi}$. By noticing that :

$$\begin{cases} \vec{r} = \sin(\theta)\cos(\phi)\vec{x} + \sin(\theta)\sin(\phi)\vec{y} + \cos(\theta)\vec{z} \\ \vec{\theta} = \cos(\theta)\cos(\phi)\vec{x} + \cos(\theta)\sin(\phi)\vec{y} - \sin(\theta)\vec{z}\,. \\ \vec{\phi} = -\sin(\phi)\vec{x} + \cos(\phi)\vec{y} \end{cases} \quad (7)$$

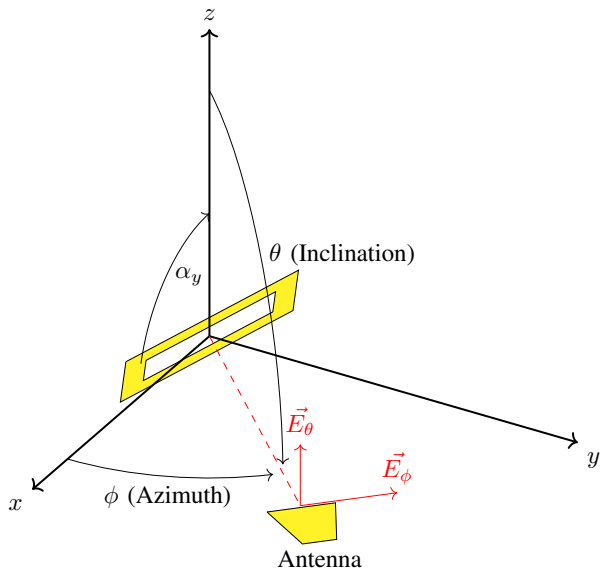

Fig. 29. Loop scatterer, coordinate system and notations considered in section VIII. The antenna is placed considering the angles θ and ϕ. The resonator is placed in the xOz plane and rotates around the $\vec{y}$ direction with an angle α_y.

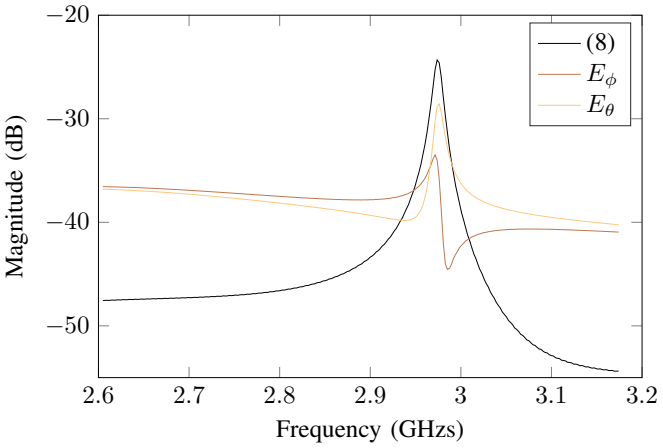

Fig. 30. Simulated S-parameters on a loop resonator with $\alpha_y = 45°$ with an incoming wave excitation along E_θ and $\theta = \phi = 80°$.

The polarization of the loop resonator can be projected to the xOy plane using (7) and (6) can be applied. The scatterer field for the loop polarization A_l can be estimated with :

$$A_l = \frac{-E_\phi \sin(\theta) - \tan(\alpha_y)\left[\cos(\phi)\cos(\theta)E_\phi + \sin(\phi)E_\theta\right]}{\sin(\theta)\sin(\phi)}. \quad (8)$$

We can notice that (8) is not defined when θ=0 or ϕ=0. These two conditions correspond to positions for which the fundamental mode of the loop is not excited by the antenna (whatever α_y), so it is not possible for these angles to recover the tag identifier. Unlike the reading at normal incidence (θ=90 or ϕ=90) where the method always allowed to recover alpha, we see here that there are positions of the antenna relative to the tag for which the measurement is not possible. However, when the antenna excites the tag resonant mode, the reading is possible, and the method once applied will improve the results

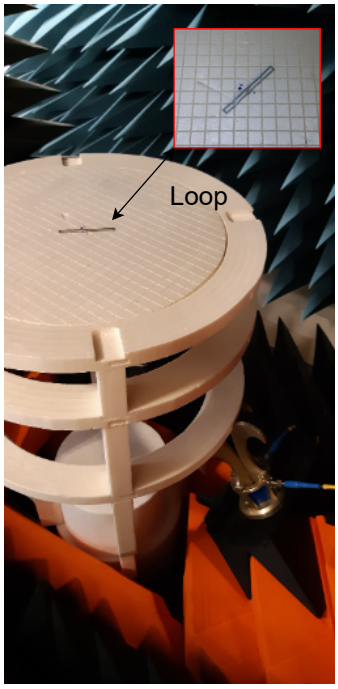

Fig. 31. Measurement setup to validate (8). The antenna is placed at $\theta = 90°$ and $\phi = 80°$. The loop is rotated with $\alpha_y = 45$.

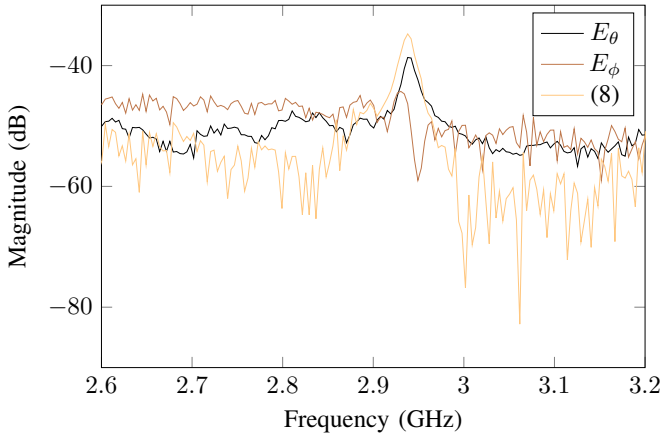

Fig. 32. Measured S-parameters on a loop resonator with $\alpha_y = 45°$ with an incoming wave excitation along E_θ.

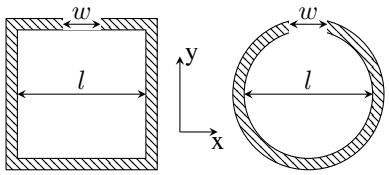

Fig. 33. Square and circular resonator topology.

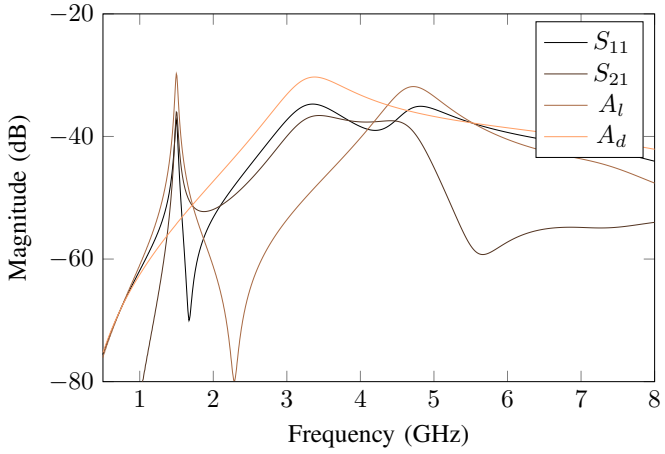

Fig. 34. Square resonator topology frequency response for $\alpha = 40°$.

on the same principle as that introduced in section II.

We also that in (7) that the loop resonator also radiates energy on the $\vec{r}$ which is not measured by the antenna. For this reason, a constant amplitude of the estimated mode for varying values of α_y is not verified there. Simulations have been done using CST MW and results for a rotation of $\alpha_y = 50°$ are plotted in Fig. 30. The antenna is arbitary placed at $\theta = \phi = 80°$. Knowing θ and ϕ, the estimation of the α_y angle is performed with the procedure described in section III. We can see once again the utility of the approach with a residual environment reduced by 25dB in this example.

Measurements in a semi-anechoic chamber were done to validate (8). The measurement setup is shown in Fig. 31 and results in Fig. 32. We can see that the peak amplitude is increased by almost 5dB but most importantly, the dipole mode of the loop is reduced by almost 10dB hence confirming the approach.

IX. Generalization of the Approach to Other Resonators and Comparison with Classical Reading Approaches

A. Example With Other Resonator's Shapes

The same concept can be applied to different types of scatterers. In this section, resonators without ground plane illustrated in Fig. 33 will be used as different examples. These resonators can be found in different works such as in [37]. Simulations have been done as in section IV. For the square loop, dimensions were $l = 25$mm, $w = 1.4$mm. For the circular loop, the same l and w were kept. Results are displayed in Fig. 34 and Fig. 35 respectively for the rectangular and circular resonators.

We can see that the highest Q-factor mode for these resonator shape is well extracted, again with an amplitude higher than the one given by S-parameters. Once again, this shows the advantage of (6) over raw measurements. This method is straight-forward for resonators with no ground plane so the following section will discuss about resonators with ground plane where additional considerations have to be taken into account.

B. Applications to Resonators With Ground Plane

In this section a resonant scatterer-based microstrip transmission-line (TL) is considered. In its simplest form, the scatterer is a metallic strip (a short-circuited dipole) above a ground plane. This scatterer can be considered as a microstrip

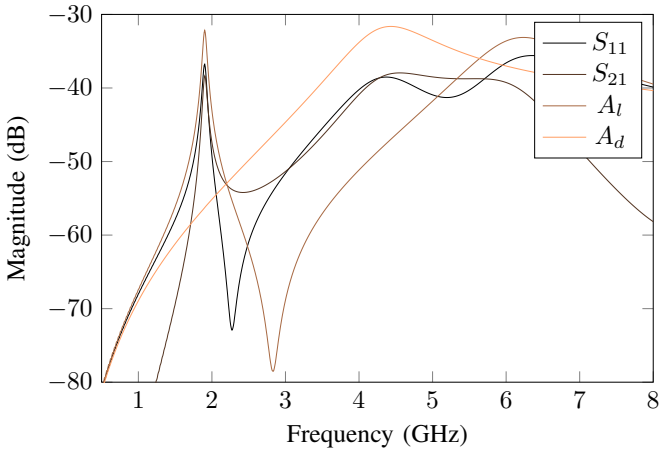

Fig. 35. Circular resonator topology frequency response for $\alpha = 50°$.

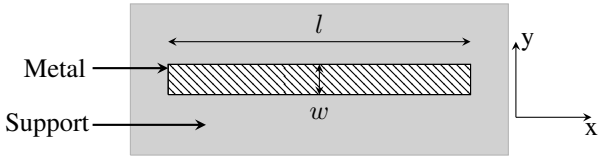

Fig. 36. Resonant scatterer-based microstrip TL. Below the dielectric support of height h a ground plane is placed. The polarization of the electric field used to excite the resonator is along x direction.

line terminated at both ends by an open circuit. This resonator is illustrated in Fig. 36.

These scatterers have a high Q-factor (around 120 at 3GHz) but due to the presence of the ground plane, these scatterers also exhibit a strong quasi-optic reflexion (comparable to the A_d mode discussed for the loop) making them hard to read. For this reason, this resonator is commonly placed at $\alpha = 45°$ and measured using cross-polarization (S_{21}) to reduce the ground response contribution. As a consequence, the reading of such tags can only be done for a fixed orientation (limiting its usage in real applications) but also the resonator signal backscattered on the co-polarization (S_{11}) is not used. In Section V, the highly reflective support was removed using an empty measurement of the metallic plate. This method being hard to implement in practice, in this section, the use of both (6) and TG jointly is presented to improve the measurements. The angle α can still be known apriori or estimated as presented in section IIV. The TG will allow to remove the ground plane response and then (6) can be applied on the TG responses to retrieve more signal using both polarizations. CST MW simulations with the tag illustrated in Fig. 36 have been done and are plotted in Fig. 37.

We can see the presence of the ground plane on the raw S-parameters with the low prominence of the resonance peak. The responses of TG allowed to increase the peak prominence by removing successfully the ground plane response. Then when (6) is applied on TG, the peak amplitude is even higher by 6dB. Note that while the TG responses are dependent of the orientation of the resonator, when (6) is applied on TG, the response is no longer orientation dependent as shown in previous sections. Measurements using the test-bench presented

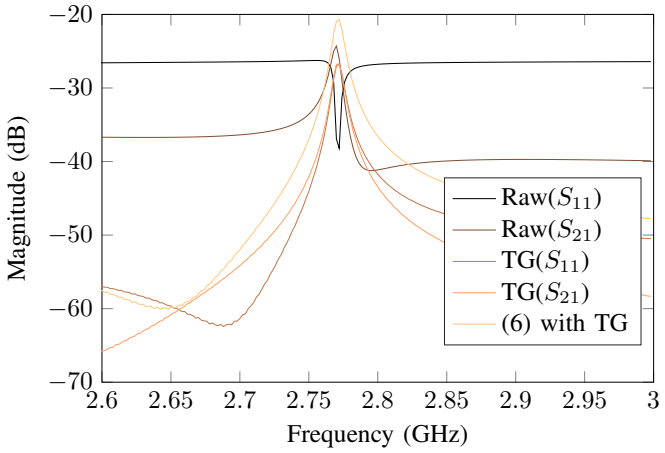

Fig. 37. Raw S-parameters and post-processed S-parameters [with TG and (6) with TG] for a microstrip resonator with $\alpha_y = 45°$.

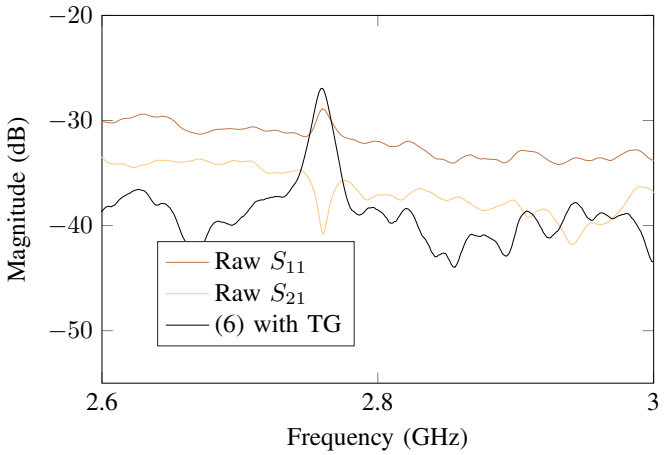

Fig. 38. Measured raw S-parameters and post-processed S-parameters [(6) with TG] for a microstrip resonator with $\alpha_y = 45°$.

in Fig. 31 are used with the microstrip resonator of Fig. 36. Raw S-parameters as well as (6) with TG are presented. The TG window is $t_{start} = 3.5e^{-9}$ and $t_{stop} = 6e^{-8}$.

C. Discussion

The method presented here allows by a projection to separate the useful signal (signal related to the loop mode) from the signal without information, namely the whole signal which is perpendicular to the excitation direction of the loop mode. It is now interesting to come back on the positioning of this method compared to the methods classically used in RFID chipless to read a tag, in particular the use of the background subtraction, the reading in cross-polarization and the time-gating. A general detailed comparison of these methods was made in the introduction of the article so the discussion here will focus on the link between these methods and the one introduced. We are interested in how these methods can interact with the introduced one in order to improve the chipless tag reading.

1) Link with the background subtraction: It is difficult in chipless to perform a tag reading without performing a

background subtraction. This can be seen from the very limited number of articles on the subject, especially when the tag is positioned next to different objects [17]. Moreover, the use of background subtraction is not necessarily prohibitive for a real application. Indeed, it is similar to calibrating the device, once the system is started. However, it should be kept in mind that if the environment changes after this calibration measurement, the system must still be able to obtain accurately the identifier, so in this case it would be necessary to perform other calibration measurements over time when the tag is not present in front of the reader antennas. So, a background subtraction calibration is compatible with the practice, however, it can only take into account the fixed part of the environment of the system, like for example the effect of the antennas (matching, coupling), and part of the direct reflections on the walls, ceiling (supposedly fixed). Even if these contributions (background subtraction relative to the fixed part of the environment) are not sufficient to allow the reading of a tag without other dedicated techniques when adding objects to the scene, a very important part of the signal not related to the tag ID is subtracted. This is why it is still preferable to use background subtraction and this is what has been done in the article.

2) Link with cross polarization reading: The objective of the introduced method is to read a classical chipless tag whatever its orientation and in order to recover the whole useful signal. This is why we use both co-polarization and cross-polarization measurements (S_{11} and S_{21} in [5]). This method is different from a classical cross-polarization measurement and therefore cannot be combined together. Compared to a co-polarization measurement, cross-polarization reading is still very efficient in that it reduces the signal by about 25 dB (to keep only the part containing the tag information). However, except for very special tag designs (with a rotation invariant cross-polarization), the reader antennas must be oriented in a specific way with respect to the environment and similarly for the tag with respect to the antennas [11]. Furthermore, unlike the approach introduced here, a cross-polarization measurement only recovers a quarter of the power of the useful signal and this for an optimal orientation of the tag with respect to the antennas. Finally, we can see from the two examples presented here (rectangular loop and microstrip dipole) that the cross-polarization measurement alone is not sufficient. If we take the rectangular loop with an optimal position (45°) for this type of reading, according to (6) we have S_{21} equal to $(A_d + A_l)/2$ which shows that we are not able to isolate the useful signal, namely A_l. Similarly, for the tag with microstrip dipole, the ground plane can have a cross-polarization reflection which will be visible on the S_{21} parameter. This is exactly what we have in Fig. 38, where the Raw S_{21} curve shows a dip (and not a peak) characteristic of the presence of a significant reflection not related to the resonance of the tag (quasi optic reflexion). In conclusion, we can say that the cross-polarization measurement is all the more interesting when used with time-gating. On its own, it does not provide an answer to all the problems of chipless reading, but it may prove indispensable in practice.

3) Link with time-gating: What allows to read a tag in a very robust way (e.g. without background subtraction in a mobile environment or with objects near the tag that potentially move), is the use of time-gating combined with a tag with a high-quality factor (higher than 100). It is precisely this idea that has been implemented in [11] and that allowed to read tags without background subtraction. We show that we can temporally separate the quasi-optical reflections of the environment from the ones linked to the resonances of the tag which is spread over more than ten nanoseconds. By optimizing the time window on which the useful signal is recovered, it is possible to read some tags in mobile environments presenting various objects. Of course, the reading in cross polarization, as it is the case for the background subtraction, improves the reading when the environment is perfectly fixed and especially can be combined with the time-gating to further improve reading. However, time-gating cannot always be applied successfully, and the rectangular loop is a very good example. Indeed, for some angles, the dipole mode will be excited, and this mode is resonant (weakly resonant, but resonant all the same) which means that temporally, it will exist over several nanoseconds, which to eliminate it would lead to use a t_{start} of the same duration and thus cut off too much of the useful signal. From then on, it would no longer be possible to read the loop mode with a sufficiently high SNR and this for a distance greater than 20cm. This example highlights one of the many interests of the proposed method. Indeed, it is quite possible to add to the described approach a time gating step (the time gating step can be performed on the raw signal as well as after the method described here, it is theoretically identical). The difference here is that the t_{start} to be considered will no longer be linked to the dipole mode (the latter will be eliminated by the method introduced in the article) but only to the environment, which means that it can be reduced to one nanosecond, for example, in order to eliminate the non-resonant part of the signal and thus keep only the part where the information is coded. This is what has been done in the article in Section VIII.

X. Conclusion

In this paper, a novel method based on polarization separation is presented to increase the peak prominence of the co-polarized chipless tag independently of the resonator orientation. We have shown how on the basis of tags already present, it is possible to read them more easily by working on the reader side by improving the post processing part. The theory has been validated in simulations and with real-life measurement with both known and unknown orientations of the resonator. The presented results highlight the potential of the approach to increase the reading robustness. In addition, this approach also allows the orientation of the tag to be determined, which provides additional information that can be used for sensor applications. The improvement was also quantified in terms of maximum reading distance. It has been seen that in some cases, a gain of 33% in the read range has been obtained compared to established TG approach. Indeed, a comparison with the commonly used TG technique is presented as well

as the jointly use of both methods to harsh environments. The ability to increase the reading robustness, the reading range as well as to detect the orientation of the tags are important elements for the practical implementation of the solution in logistics for example.

ACKNOWLEDGMENT

The authors are also thankful towards Ms. Nathalie Franck for her help in proofreading the paper.

REFERENCES

[1] M. R. Rieback, B. Crispo, and A. S. Tanenbaum, "The evolution of RFID security," *IEEE Pervasive Comput.*, no. 1, pp. 62–69, 2006.
[2] P. Nikitin, "Leon Theremin (lev termen)," *IEEE Trans. Antennas Propag.*, vol. 54, no. 5, pp. 252–257, 2012.
[3] G. Brooker and J. Gomez, "Lev termen's great seal bug analyzed," *IEEE Aerosp. Electron. Syst. Mag.*, vol. 28, no. 11, pp. 4–11, 2013.
[4] J. Landt, "The history of RFID," *IEEE potentials*, vol. 24, no. 4, pp. 8–11, 2005.
[5] A. N. Nambiar, "RFID technology: A review of its applications," in *Proceedings of the world congress on engineering and computer science*, vol. 2. Citeseer, 2009, pp. 20–22.
[6] J. Kracek, M. Svanda, and K. Hoffmann, "Scalar method for reading of chipless rfid tags based on limited ground plane backed dipole resonator array," *IEEE Trans. Microw. Theory Tech.*, vol. 67, no. 11, pp. 4547–4558, 2019.
[7] M. Polivka, J. Havlicek, M. Svanda, and J. Machac, "Improvement in robustness and recognizability of rcs response of u-shaped strip-based chipless rfid tags," *IEEE Antennas and Wireless Prop. Lett.*, vol. 15, pp. 2000–2003, 2016.
[8] N. C. Karmakar, E. M. Amin, and J. K. Saha, *Chipless RFID sensors*. Wiley Online Library, 2016.
[9] E. Perret, *Radio frequency identification and sensors: from RFID to chipless RFID*. John Wiley & Sons, 2014.
[10] A. Ramos, Z. Ali, A. Vena, M. Garbati, and E. Perret, "Single-layer, flexible, and depolarizing chipless RFID tags," *IEEE Access*, vol. 8, pp. 72 929–72 941, 2020.
[11] A. Ramos, E. Perret, O. Rance, S. Tedjini, A. Lázaro, and D. Girbau, "Temporal separation detection for chipless depolarizing frequency-coded RFID," *IEEE Trans. Microw. Theory Tech.*, vol. 64, no. 7, pp. 2326–2337, 2016.
[12] S. Hu, Y. Zhou, C. L. Law, and W. Dou, "Study of a uniplanar monopole antenna for passive chipless uwb-rfid localization system," *IEEE Trans. Antennas Propag.*, vol. 58, no. 2, pp. 271–278, 2009.
[13] D. Girbau, A. Lázaro, and Á. Ramos, "Time-coded chipless rfid tags: Design, characterization and application," in *2012 IEEE International Conference on RFID-Technologies and Applications (RFID-TA)*. IEEE, 2012, pp. 12–17.
[14] R. B. Green, *The general theory of antenna scattering*. The Ohio State University, 1963.
[15] R. Rezaiesarlak and M. Manteghi, "Complex-natural-resonance-based design of chipless rfid tag for high-density data," *IEEE Trans. Antennas Propag.*, vol. 62, no. 2, pp. 898–904, 2013.
[16] C. E. Baum, "On the singularity expansion method for the solution of electromagnetic interaction problems," AIR FORCE WEAPONS LAB KIRTLAND AFB NM, Tech. Rep., 1971.
[17] A. T. Blischak and M. Manteghi, "Embedded singularity chipless RFID tags," *IEEE Trans. Antennas Propag.*, vol. 59, no. 11, pp. 3961–3968, 2011.
[18] Z. Ali, E. Perret, N. Barbot, and R. Siragusa, "Extraction of aspect-independent parameters using spectrogram method for chipless frequency-coded RFID," *IEEE Sensors J.*, vol. 21, no. 5, pp. 6530–6542, 2020.
[19] A. Vena, E. Perret, and S. Tedjini, "Design of compact and auto-compensated single-layer chipless rfid tag," *IEEE Trans. Microw. Theory Tech.*, vol. 60, no. 9, pp. 2913–2924, 2012.
[20] O. Rance, R. Siragusa, P. Lemaître-Auger, and E. Perret, "Contactless characterization of coplanar stripline discontinuities by RCS measurement," *IEEE Trans. Antennas Propag.*, vol. 65, no. 1, pp. 251–257, 2016.
[21] F. Requena, M. Gilch, N. Barbot, D. Kaddour, R. Siragusa, F. Costa, S. Genovesi, and E. Perret, "Thermal modeling of resonant scatterers and reflectometry approach for remote temperature sensing," *IEEE Trans. Microw. Theory Tech.*, vol. 69, no. 11, pp. 4720–4734, 2021.
[22] F. Requena, N. Barbot, D. Kaddour, and E. Perret, "Chipless RFID temperature and humidity sensing," *in 2021 IEEE MTT-S International Microwave Symposium*, 2021.
[23] F. Costa, D. Brizi, S. Genovesi, A. Monorchio, G. Manara, F. Requena, and E. Perret, "Wireless detection of water level by using spiral resonators operating in sub-ghz range," in *2019 IEEE International Conference on RFID Technology and Applications (RFID-TA)*. IEEE, 2019, pp. 197–200.
[24] A. M. J. Marindra and G. Y. Tian, "Chipless RFID sensor tag for metal crack detection and characterization," *IEEE Trans. Microw. Theory Tech.*, vol. 66, no. 5, pp. 2452–2462, 2018.
[25] E. M. Amin, R. Bhattacharyya, S. Sarma, and N. C. Karmakar, "Chipless RFID tag for light sensing," in *2014 IEEE Antennas and Propagation Society International Symposium (APSURSI)*. IEEE, 2014, pp. 1308–1309.
[26] M. Polivka, J. Havlicek, M. Svanda, and J. Machac, "Improvement in robustness and recognizability of RCS response of u-shaped strip-based chipless RFID tags," *IEEE Antennas and Wireless Prop. Lett.*, vol. 15, pp. 2000–2003, 2016.
[27] M. Borgese, S. Genovesi, G. Manara, and F. Costa, "Radar cross section of chipless RFID tags and BER performance," *IEEE Trans. Antennas Propag*, vol. 69, no. 5, pp. 2877–2886, 2020.
[28] M. Khaliel, A. El-Awamry, A. Fawky, M. El-Hadidy, and T. Kaiser, "A novel co/cross-polarizing chipless RFID tags for high coding capacity and robust detection," in *2015 IEEE international symposium on antennas and propagation & USNC/URSI national radio science meeting*. IEEE, 2015, pp. 159–160.
[29] N. Barbot, O. Rance, and E. Perret, "Chipless RFID reading method insensitive to tag orientation," *IEEE Trans. Antennas Propag.*, vol. 69, no. 5, pp. 2896–2902, 2020.
[30] S. Genovesi, F. Costa, F. A. Dicandia, M. Borgese, and G. Manara, "Orientation-insensitive and normalization-free reading chipless RFID system based on circular polarization interrogation," *IEEE Trans. Antennas Propag.*, vol. 68, no. 3, pp. 2370–2378, 2019.
[31] O. Rance, N. Barbot, and E. Perret, "Design of planar resonant scatterer with roll-invariant cross polarization," *IEEE Trans. Microw. Theory Tech.*, vol. 68, no. 10, pp. 4305–4313, 2020.
[32] R. Olivier, B. Nicolas, and P. Etienne, "Comparison between cross-polarization and circular polarization interrogation for robust chipless rfid reading," *51th European Microwave Conference (EuMC 2021)*, 2021.
[33] R. Rezaiesarlak and M. Manteghi, *Chipless RFID*. Springer, 2016.
[34] C. A. Balanis, *Antenna theory: analysis and design*. John wiley & sons, 2015.
[35] E. F. Knott, J. F. Schaeffer, and M. T. Tulley, *Radar cross section*. SciTech Publishing, 2004.
[36] N. Barbot, O. Rance, and E. Perret, "Classical RFID versus chipless RFID read range: Is linearity a friend or a foe?" *IEEE Trans. Microw. Theory Tech.*, 2021.
[37] A. Vena, E. Perret, and S. Tedjini, "A compact chipless RFID tag using polarization diversity for encoding and sensing," in *2012 IEEE International Conference on RFID (RFID)*. IEEE, 2012, pp. 191–197.